Arabian Journal of Chemistry (2023) **16**, 104419

King Saud University

Arabian Journal of Chemistry

www.ksu.edu.sa
www.sciencedirect.com

ORIGINAL ARTICLE

Anticancer and microbicide action of carbon quantum dots derived from microcrystalline cellulose: Hydrothermal versus infrared assisted techniques

Amal T. Mogharbel [a], Sraa Abu-Melha [b], Ahmed Hameed [c], Roba M. S. Attar [d], Abdulmajeed F. Alrefaei [e], Albandary Almahri [f], Nashwa El-Metwaly [c,*]

[a] *Department of Chemistry, College of Science, University of Tabuk, 71474 Tabuk, Saudi Arabia*
[b] *Department of Chemistry, Faculty of Science, King Khalid University, Abha 62529, Saudi Arabia*
[c] *Department of Chemistry, Faculty of Applied Sciences, Umm Al-Qura University, Makkah, Saudi Arabia*
[d] *Department of Microbiology, Faculty of Science, University of Jeddah, P.O. Box 2360S, Saudi Arabia*
[e] *Department of biology/Genetic and Molecular Biology Central Laboratory (GMCL), Jamoum University College, Umm Al Qura University, Makkah 2203, Saudi Arabia*
[f] *Department of Chemistry, College of Science and Humanities in Al-Kharj, Prince Sattam Bin Abdulaziz University, Al-Kharj 11942, Saudi Arabia*

Received 18 July 2022; accepted 8 November 2022
Available online 14 November 2022

KEYWORDS

MCC;
CQDs;
Hydrothermal conditions;
Infrared assisted technique;
Anticancer;
Microbicide laborer

Abstract Urgent requirement for medication from cancer diseases and different microbial infections is interestingly considered. Carbon quantum dots (CQDs) as environmentally friendly fluorescent carbon nano-functionalized materials are popularly considered for application in medical purposes. Herein, a comparative study is presented for the affinity of CQDs ingrained from microcrystalline cellulose (MCC) prepared under hydrothermal conditions (CQDs-HT) versus that prepared under infrared assisted technique (CQDs-IR) for acting as anticancer and antimicrobial laborers. The estimated size averages for the obtained CQDs-HT & CQDs-IR were 7.8 & 9.8 nm, respectively. CQDs-HT showed rationally higher anti-proliferative action against Hepatocellular Carcinoma (HepG2) compared to CQDs-IR. Treatment with 1000 µg/mL of CQDs-IR & CQDs-HT exhibited 78 & 90 % mortality percentage of cancer cells, respectively. The obtained CQDs showed excellent microbicide potentiality and the minimum inhibitory concentration

* Corresponding author.
E-mail address: nmmohamed@uqu.edu.sa (N. El-Metwaly).
Peer review under responsibility of King Saud University.

Production and hosting by Elsevier

https://doi.org/10.1016/j.arabjc.2022.104419

(MIC) from the synthesized CQDs-TH and CQDs-IR was ranged in 100–350 μg/mL and 300–400 μg/mL against different pathogens including bacteria and fungi, respectively. As a conclusion, hydrothermal technique showed seniority over infrared assisted technique in nucleation of CQDs with higher anticancer and microbicidal activities.

1. Introduction

Carbon Quantum Dots (CQDs) were superiorly investigated as carbon nanoparticles (Wang et al., 2017), to be exhibited with particle size less than or equal to ten nanometers, whereas, graphene nano-sheets are characterized with planer size less than one hundred nanometers and were identified as graphene quantum dots (GQDs) (Dong et al., 2014). Compared to the well-known quantum dots with semiconducting properties, unique characters of CQDs are their chemical inertness, biocompatibility, low toxicity, low cost, and exhibited superior fluorescent activity of semiconductor quantum dots (Lim et al., 2015). CQDs are described in term of a surface-employed carbon-based core, whereas, CQDs are quasi-circular carbon nanoparticles composed of crystalline or amorphous centers with graphite carbon (sp^2 carbon) or graphene-oxide sheets blended via diamond-like sp^3 hybridized carbon structures (Wang et al., 2017; Lim et al., 2015; Wang and Hu, 2014). Simultaneously, CQDs are mostly composed of hetero atoms containing accessible groups on their terminal sides that facilitate their solubility in different solvents and improving their potentiality for different applications compared to the other carbon-based nanomaterials. Owing to their unique structure and characters, CQDs are advantageous with unique characters like their tunable photoluminescence (PL), distinctive photo-motivated electron transferring, their effective absorption for the photovoltaic irradiation, and their IR-response for up-interchanged photoluminescent property (Wang et al., 2017; Lim et al., 2015; Wang and Hu, 2014).

Different approaches were interestingly concerned with the innovation of different synthetic techniques for synthesis of size and geometrically controlled CQDs, whereas, hydrothermal treatment (Qu et al., 2012), electrochemical oxidation (Li et al., 2010), ultrasonic treatment (Li et al., 2011), and laser irradiation (Sun et al., 2006) are known to be the most commonly applicable techniques for clustering of CQDs. Some of these techniques are disadvantageous with complexity, expensiveness and low quantum yields. Therefore, as an important issue, researchers were challenged for modification of such mentioned techniques to be lesser in cost, time and energy saving for synthesis of CQDs with high quantum yield to be applicable in larger scale. Hydrothermal method is one of the appropriate synthetic approaches for preparation of carbon quantum dots that can produce highly size regulated CQDs from various resources of organic molecules and carbohydrates (Barati et al., 2015). The biocompatibility and non-toxicity of CQDs as prerequisite characters for their applicability in different biomedical purposes leading to be uniquely innovated for their application in treatment of cancer. Some of researching approaches were encouraged to be studied for the CQDs bio-toxic effects on various cancer cells like, Hep-2 (Wu et al., 2014), HeLa (Fan et al., 2014) and A549 (Wu et al., 2013; Sachdev and Gopinath, 2015). Moreover, it was confirmed that, different green synthesized CQDs were exhibited with both of superior fluorescent properties and bioactivity such as anti-oxidizing, antitumor and anti-inflammatory properties. Hsu et al., studied the affinity of photoluminescent CQDs ingrained from green tea for extremely high inhibition activity toward cancer cells. Also, Zhao et al., studied the green synthesizing of fluorescent CQDs from garlic for bio-imaging and free radical scavenging. Vasimalai et al, reported another green synthetic methodology for preparation of optically active CQDs from spices for bio-imaging and inhibition the growth of cancer cells. Li et al, investigated another green synthetic technique of Fluorescent CQDs derived from chitosan derivatives with studying the bio-distribution, cytotoxicity, and antioxidant action. Additionally, Xu et al, studied the affinity of aspirin-based carbon dots, as a good biocompatible material applied for bio-imaging with anti-inflammation action (Hsu et al., 2013; Zhao et al., 2015; Vasimalai et al., 2018; Li et al., 2018; Xu et al., 2016).

On the other hand, numerous of microbicide reagents i.e., antiseptic and disinfecting reagents were exploited for inactivating microorganisms to prevent their risky infection (Emam et al., 2019; Emam et al., 2017; Ahmed et al., 2019; Emam et al., 2018), but, such types of the microbicide reagents are known to be disadvantageous with their toxicity, leading to high dangerous healthy problems such as contact dermatitis and irritation. Additionally, some of the microbial strains could adapt and exhibit resistant versus such laborers by time (Pidot et al., 2018). Therefore, the exploitation of CQDs as alternative microbicide laborers with superior antimicrobial performance and low toxicity was extensively considered. As challengeable way, the presented work is focused on studying the affinity of hydrothermal versus infrared assisted techniques for ingraining of size/shape controlled CQDs from microcrystalline cellulose (MCC) as hydroxyl containing biopolymers. Moreover, the current approach is considered with the preparation of CQDs via the mentioned green synthetic methodology to be concurrently applicable as anticancer and microbicide laborers. According to our knowledge, no approaches in literature were considered with presenting of comparative overview for monitoring of the effect of variation in the synthetic techniques on the anticancer and antimicrobial affinity of the ingrained CQDs. Additionally, ingraining of CQDs is extensively considered without the requirement of any toxic organic solvents, to be biocompatible for exploitation in the biomedical fields. Successive ingraining of CQDs via the exploitation of MCC under the hydrothermal versus infrared assisted techniques was affirmed via several instrumental analyses like, UV–Visible spectroscopy, Transmission Electron Microscopy, FTIR, ^{1}H NMR and ^{13}C NMR. Afterword, the fluorescent properties of the ingrained CQDs were also followed up. The microbicide potency of the prepared CQDs was confirmed via inhibition zone method. Moreover, the anticancer potentiality of the synthesized CQDs was examined via WST-1 cell proliferation assay for monitoring their antitumor effects against Hepatocellular Carcinoma (HepG2) for CQDs prepared via hydrothermal (CQDs-HT) versus infrared assisted (CQDs-IR) techniques.

2. Experimental work

2.1. Materials and chemicals

Microcrystalline cellulose (MCC, Avicel®PH-101, particle size of ~ 50 μm) and NaOH (sodium hydroxide 99 %) were obtained from Merck, Darmstadt–Germany. They were both used as received and the colloidal solutions were prepared using the deionized water.

2.2. Ingraining of CQDs from MCC

10 & 30 g/L MCC were hydrolyzed with 10 g/L of NaOH and subsequently the colloidal solutions were magnetically stirred for 2 h at 90℃. Afterward, the mixture solutions were trans-

ferred to vertical hydrothermal autoclave reactor and then left in oven or infrared assisted conditions (Infra-Color Dyeing Machine – from India) at 125 ℃ for 6 h to complete the nucleation of CQDs. The autoclave reactor was cooled at room temperature and the color of solution was turned to dark brown after treatment. The contents in the autoclave reactors were centrifuged for 15 min at 5000 rpm using Hermile Z326 K centrifuge to separate the insoluble particles. To obtain ultrafiltered/mono-dispersed CQDs, the dispersed solutions were then dialyzed with distilled water using pure-A-lyzer dialysis kits with 6–8 kDa from Sigma-Adrich.

2.3. Instrumental analyses and CQDs characterization

Absorption spectral data for MCC and the ingrained CQDs were manifested using Cary 100 UV–vis, UV–Vis-NIR spectrophotometer in wavelength range of 250–750 nm, from Agilent. Topographicalfeatures and size average of the ingrained CQDs were investigated using JEOL-JEM-1200 High Resolution Transmission Electron Microscope (from Japan). The size average of CQDs was evaluated by 4 pi analysis software (from USA) for 50 particles. Zeta-potential was measured for the ingrained CQDs by using the Zetasizer analyzer (Malvern Zeta-sizer Nano ZS, Malvern Instruments ltd – from UK). The measurements were carried out in isolated chamber at 25 °C using the dynamic light scattering (DLS) technique. Infrared spectral mapping data were obtained using Jasco FT/IR 6100 spectrometer. The absorbance was also detected at 500 – 4000 cm^{-1}, using 15 points smoothing, 4 cm^{-1} resolution, 64 scanning times with scanning rate of 2 $mm.sec^{-1}$, on Jeol-Ex-300 NMR spectrometer (JEOL – Japan), the spectral results of nuclear magnetic resonance (^{1}H NMR and ^{13}C NMR) were estimated. In ultraviolet–visible spectral range using Spectro-fluorometer (JASCO FP8300), photoluminescence spectral data for CQDs were collected. At room temperature and with excitation at 340 nm, the measurements were carried out, and similarly, the emission was detected at room temperature.

2.4. Cell proliferation assay and antitumor affinity

Comparative study between ingraining of CQDs under hydrothermal conditions and infrared assisted technique for nucleation of cytotoxic/ anticancer CQDs with mortal effects against Hepatocellular Carcinoma (HepG2) was estimated with WST-1 assay. Hepatocellular Carcinoma (HepG2) cell line was collected by Nawah Scientific Inc. (Mokatam, Cairo, Egypt). Cells were suspended in DMEM media supplemented with 100 mg/ml of streptomycin, 100 units/ ml of penicillin and 10 % of heat-inactivated fetal bovine in humidified, 5 % (v/v) CO_2 atmosphere at 37 ℃. Cell mortality was estimated in WST-1 assay using Abcam®kit (ab155902WST-1Cell Proliferation Reagent). Aliquots of 50 µL cell dispersion ($3x10^3$ cells) were ingrown in 96-well plates and incubated in media for 24 h. Cells were cured with another aliquot of 50 µL media containing CQDs at serial concentrations (10 – 100 ug/ml). After 48 h of exposure to CQDs, cells were treated with 10 µL WST-1 laborer and the absorption was estimated after one hour at 450 nm using a BMG LABTECH®- FLUOstar Omega microplate reader (Allmendgrün, Ortenberg) (Alaufi et al., 2017; Sharma et al., 2014).

2.5. Microbicide potentiality

Microbicide potentiality of the ingrained CQDs against selected pathogenic species was tested via the qualitative method of inhibition zone (Kováčová et al., 2018; Kováčová et al., 2020). In this test, three different microbial species of gram-positive bacteria species (*Bacillus cereus & Staphylococcus aureus*), gram-negative bacteria species (*Escherichia coli*) and fungal species (*Candida albicans*) were examined. To estimate the lowest concentration of the prepared CQDs which exhibited an observable inhibition in microbial growing, the minimal inhibitory concentration (MIC) from CQDs colloid was measured. In the inhibition zone technique (disk diffusion test), different examined bacterial series were grown in the medium for preparing the microbial suspension. 100 µL of microbial suspension was diffused on the agar plate corresponded for broth in which it was maintained. 10 µL of CQDs was dropped in the middle of the plate to be incubated at 37 °C for one day. The diameter of the inhibition zone was estimated in millimeters using slipping calipers according to CLSI (2012). For determining of MIC, series of diluted solutions of the prepared CQDs (0 – 1000 µL/mL) were prepared to be dropped into the testing plates. After incubating at 37 °C for one day, the colony forming units (CFU) were counted for each diluted colloid (Emam et al., 2017; CLSI, 2012).

3. Results and discussion

3.1. Mechanism for synthesis of lipophobic CQDs

MCC macromolecules were successively exploited for clustering lipophobic CQDs under the hydrothermal conditions at alkaline pH as schematically plotted in Fig. 1. The reaction mechanism for nucleation of CQDs from alkali dissolved MCC could be elucidated as follows: firstly MCC polymeric blocks are supposed to be alkali-decomposed and fragmented, to be sequentially under the hydrothermal conditions or under the effect of infrared irradiation, re-polymerized, aromatized and eventually oxidized, for clustering of the required size and shape controlled CQDs (Li et al., 2011). For ultra-filtration, dialysis was performed for production of the mono-dispersed/highly purified CQDs with regulated geometrical features (Li et al., 2011). Moreover, MCC macromolecular structure is suggested to be depolymerized under the strong alkaline conditions to its repeating units of glucose, whereas, furfural intermediates are hypothesized to be produced under the hydrothermal conditions (Ryu et al., 2010; Kwon et al., 2012), that in turn is supposed to be polymerized and aromatized to aromatic oxygen containing polymers (Sakaki et al., 1996; Chen et al., 2013). Fig. 1 showed the interchanging in the color of the prepared solution of CQDs, whereas, the color was changed from white to yellow colored solution for alkali treated MCC after heating for 30 min at 100 °C. The color was turned to brownish yellow after prolonging the time of heating to one hour, and observably changed to reddish brown after exposing to hydrothermal/infrared conditions (125 °C for 6 h), whereas, it lastly changed to pale yellow after dialysis.

3.2. Characterization of CQDs

UV–Visible spectroscopic data for the prepared colloids of CQDs that were produced via the exploitation of MCC with

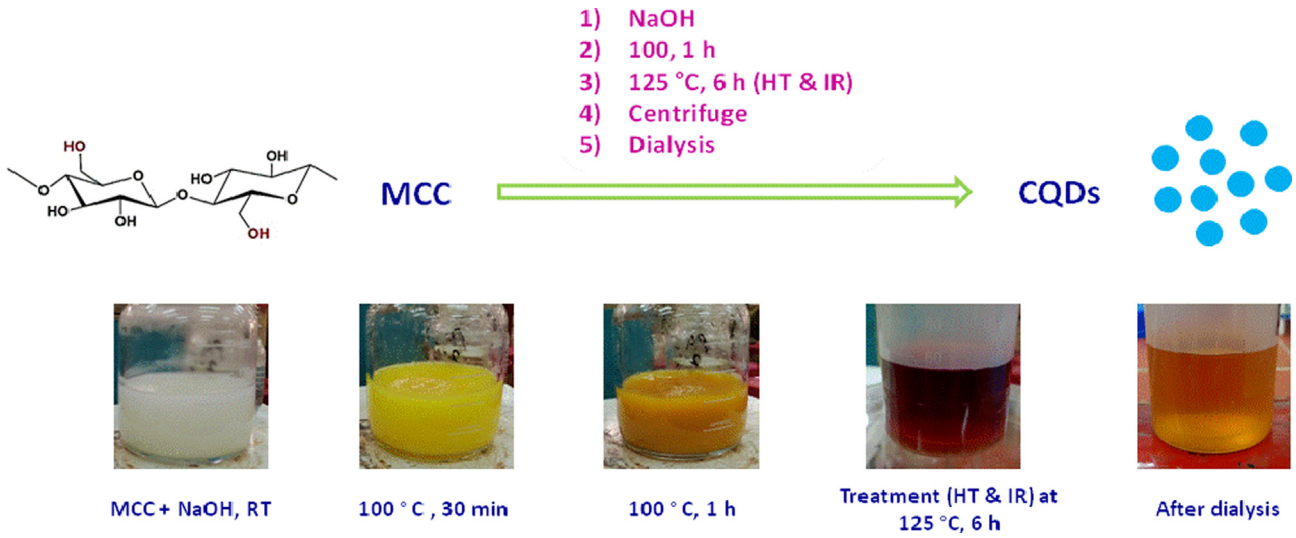

Fig. 1 Scheme for synthesis of CQDs from MCC by hydrothermal and infrared treatment.

two different concentrations (1 % & 3 %) were plotted in Fig. 2. While Fig. 2**a**, showed the spectral results of CQDs clustered from MCC under hydrothermal conditions and Fig. 2**b** represented the spectral data of CQDs nucleated from MCC under the effect of infrared irradiation. The spectral mapping results showed that, regardless to the type of synthetic technique, for CQDs colloid prepared from 1 % MCC was characterized with strong absorption band at 270 nm referring to π - π* transition (assumed to be correlated to conjugative system in the aromatic nuclei) and electron radiation relaxation and broad band at 430 nm with long tail in visible region characteristic for n- π* transition (correlated to the oxygen containing functional groups) (Kim et al., 2019; Luo et al., 2009). However, raising the concentration of MCC resulted in sharpening and red shifting of the characteristic band for n - π* transition to be observed at 490 nm, whereas, the characteristic bands of π- π* transition was not affected. These findings could affirm that, the prepared CQDs could contain aromatic conjugated nature and could reflect the effect of enhancement effects of nucleating CQDs with higher degree of aromaticity and decorated with greater amounts of functional groups using higher concentration of MCC (Gao et al., 2016).

Fig. 3 presented TEM microscopic images of the colloidal solutions of the prepared CQDs via exploitation of MCC before and after dialysis, to inform about the geometry and topography of the ingrained CQDs, whereas, the size distribution of the nucleated CQDs was also estimated. The microscopic images strongly affirmed the compatibility and the superiority of MCC in nucleation of size and shape controlled CQDs, in addition to confirm the vital role of dialysis in ultrafiltration for ingraining sphere/highly mono-dispersed CQDs. Estimation of size-distribution showed that, CQDs ingrained using under hydrothermal conditions exhibited with average size of 7.8 ± 2.4 nm with d-spacing of 3.0 ± 0.3 Å (Fig. 3**a**), while, nucleation of CQDs under the effect of infrared irradiation was reflected in insignificant enlargement in the average size to be 9.6 ± 2.9 nm with d-spacing of 3.1 ± 0.4 Å (Fig. 3**b**). It could be attributed to the oxygen containing decorative groups which capped CQDs prepared from MCC, and as it is well known that, oxygen containing accessible groups were hypothesized to be superiorly exploited in conjugation and controlling of smaller sized/homogenously/well dispersed CQDs. So, it could be concluded that, the viewed images in Fig. 3 confirmed the compatibility of alkali hydrolyzed MCC in synthesis of CQDs under hydrothermal conditions to be more favorable rather than infrared assisted technique for ingraining of shape/size controllable CQDs.

Analyzing the zeta electric potential was performed in order to identify the zeta potential of the currently prepared CQDs-HT compared to CQDs-IR. Zeta potential is a key factor for the strength of repulsion or attraction between the dispersed particles in a colloidal form. The smaller are the dispersed particles, the higher is the estimated negative value of zeta potential, meaning that the more is the stability of the colloidal solution, whereas, the stable dissolution or dispersion could prevent the CQDs coagulation. It could be seen from Fig. 4, the estimated values of zeta potential were negatively charged for both of CODs-IR & CODs-HT colloids, to be − 4 to − 9 mV and average of − 6.1 mV for CODs-IR, while, it was higher negative values (-9 to − 13 mV and average of − 11.1 mV) in case of CODs-HT. This approves that, CODs-HT were exhibited with better physical stability rather than CODs-IR (Pandey et al., 2020).

3.3. NMR & FT-IR

NMR spectral mapping results were shown in **Figure S1** for successive prediction of reaction mechanism and confirmation of successive nucleation of CQDs from MCC macromolecules under hydrothermal conditions. Fig. S1**a** showed ^{1}H NMR for CQDs prepared from MCC, while, the spectrum for CQDs showed the characteristic bands for protons of sp^3 C—H at 1–2 ppm, protons of O—H at 3.5–4 ppm, protons bonded to C═O groups at 4.5–6 ppm and aromatic or sp^2 CH = CH protons at 8–8.5 ppm. Fig. S1**b** represented ^{13}C NMR spectrum of MCC based CQDs and it could be clearly notified that, the typical bands for CQDs were detected at 30 ppm corresponding to sp^3 carbons, 73 ppm signified for carbons attached with

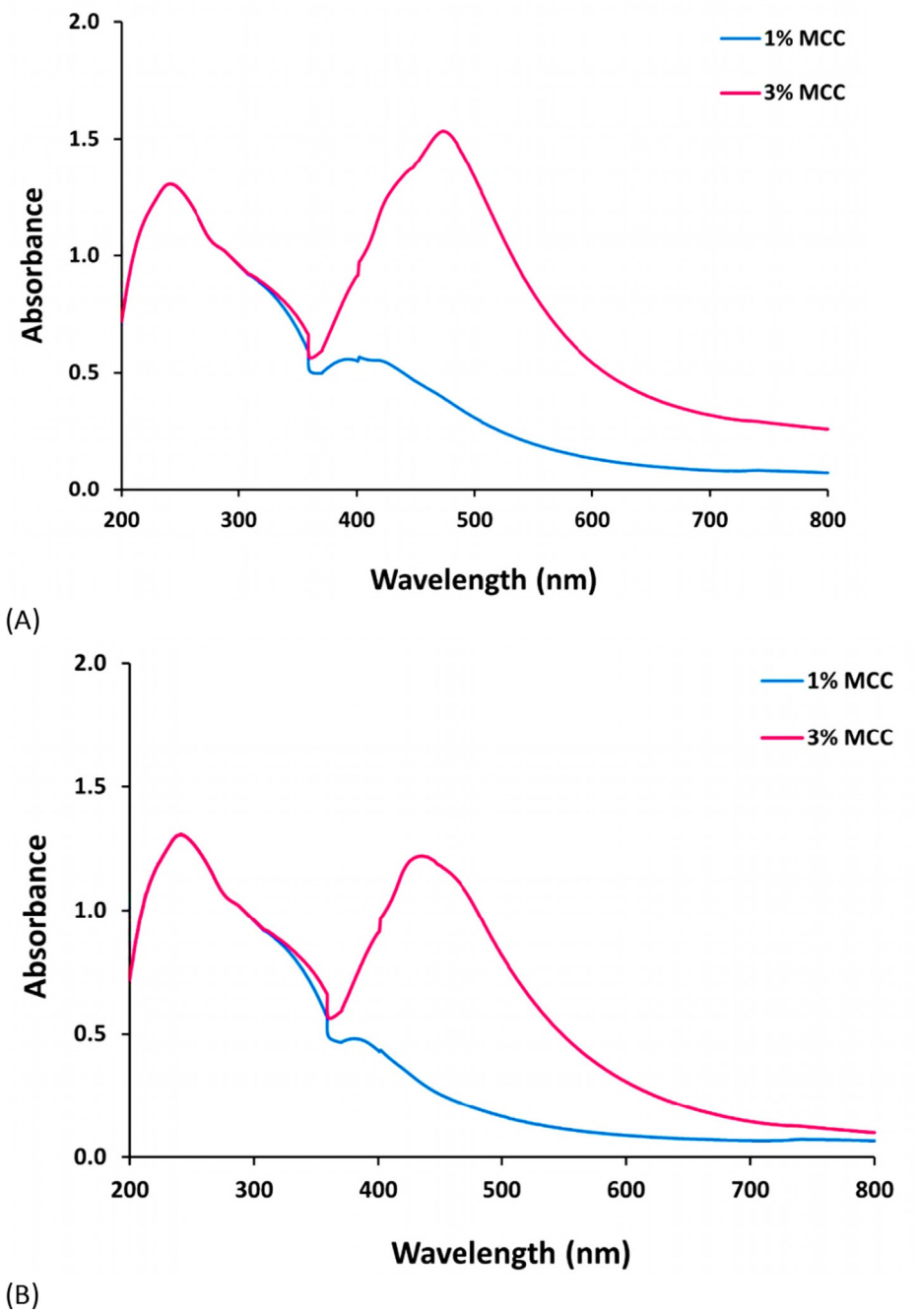

Fig. 2 Absorbance spectra for the prepared CQDs; **[a]** hydrothermal (HT) and **[b]** Infrared (IR).

hydroxyl groups, 165 ppm C═C specialized for aromatic or sp^2 carbons and 182 ppm characteristic for carbons of C═O groups (Emam and Ahmed, 2021; Emam et al., 2021).

On the other hand, **Figure S2** represents FT-IR spectrum for native MCC &CQDs prepared from alkali hydrolyzed MCC under hydrothermal conditions. **Figure S2** showed that, the native MCC exhibited characteristic spectral peaks at 3331 cm^{-1} for OH stretching, 2900 cm^{-1} for asymmetric aliphatic CH_2, stretching C═O at 1642–1649 cm^{-1} and at 1400–1300 cm^{-1} for sp^3 C—H bending. The characteristic peaks for glycoside linkage, C—O, C—O—C, and C-OH bonds were seen at 1250–1001 cm^{-1} (Kumar et al., 2010). However, after exploitation of MCC macromolecules as CQDs precursor, all the characteristic bands of MCC were detected with much lower intensity, in addition to, the characteristic bands of stretching C═O and at 1400–1300 cm^{-1} for sp^3 C—H bending were completely disappeared, and new peaks were estimated at 1406 cm^{-1} characteristic for C—C aromatic ring chain vibrations, 874 cm^{-1} and at 710 cm^{-1} that are characteristic for sp^2 C—H bending. Hence, this evidence approved the

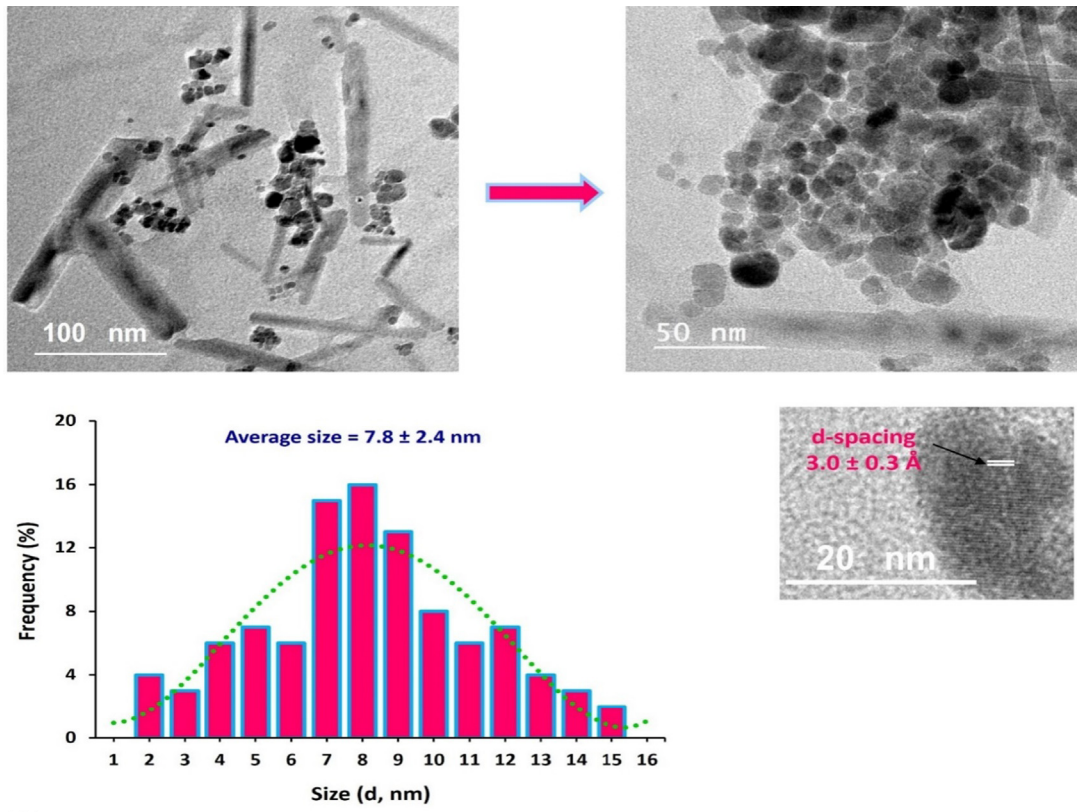

(A)

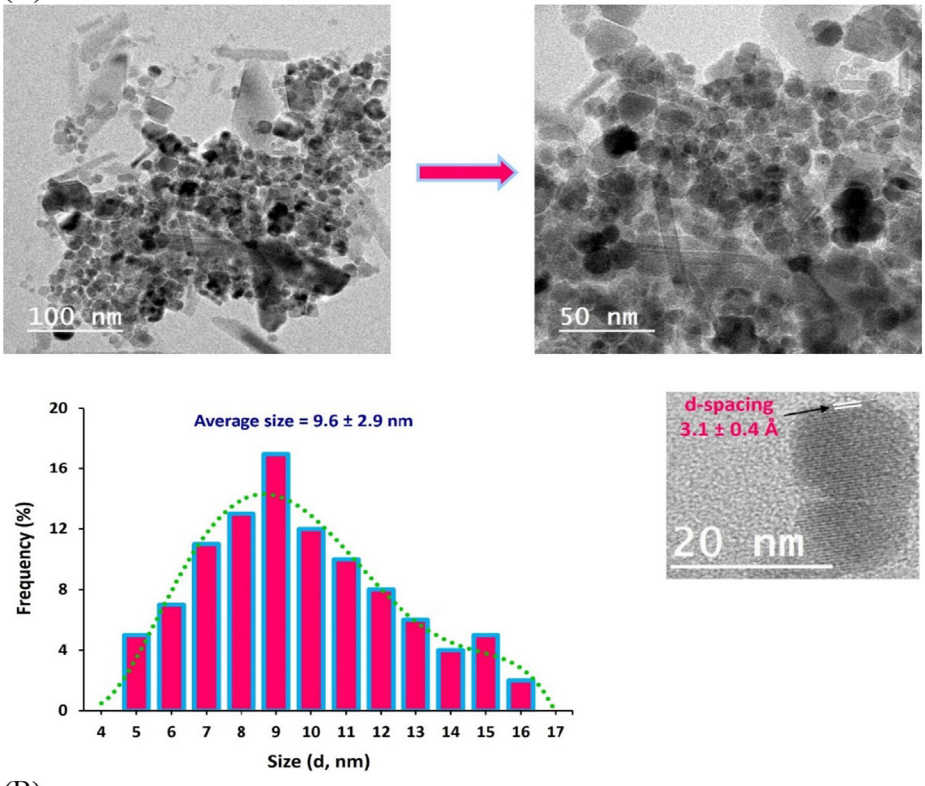

(B)

Fig. 3 TEM images for the prepared CQDs; **[a]** hydrothermal (HT) and **[b]** Infrared (IR).

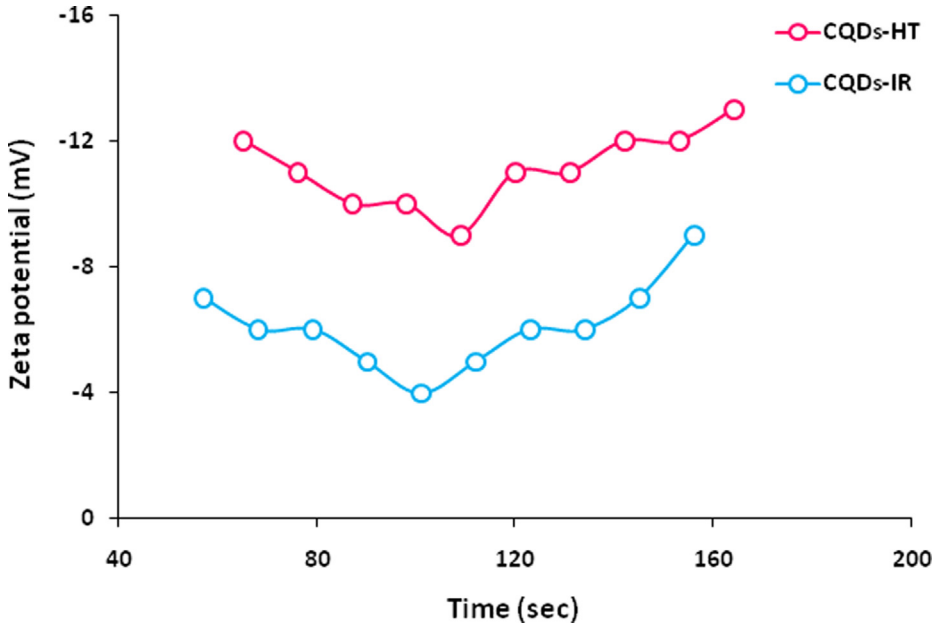

Fig. 4 Zeta-potential for the prepared CQDs.

compatibility of MCC macromolecules for generation of CQDs with oxygen containing decorative groups.

3.4. Fluorescent properties

Photoluminescent properties of CQDs were investigated to be directly reflected from the decorative functional groups rather than their size distribution (Gao et al., 2016). Wu et al. confirmed that, the photoluminescent properties of CQDs are specialized for their characteristic surface states that are structured from decorative functional groups on their carbonic building blocks (Wu et al., 2014). The surface states are the optically active centers composed from the synergetic hybridization of the surface functional groups on the carbonic cores (Zhang et al., 2010).

Therefore, the optical characters of CQDs that were currently ingrained from MMC were investigated via photoluminescence spectroscopic detection and the fluorescence emission spectral results after excitation at 370 nm and were presented in Fig. 5. Emission spectra were detected at different excitation wavelengths, in order to select wavelength range with the maximum emission, whereas, the significant highest emission is observed at 370 nm (Fig. 5a). The plotted spectra showed the excited CQDs prepared from MCC under hydrothermal (Fig. 5**a**) and infrared assisted conditions (Fig. S2**b**), before and after dialysis in order to affirm the effect of dialysis on the optical activities of the ingrained CQDs. Form the plotted data, it could be depicted that, the detection of the emission peaks in UV–visible absorption spectrum confirmed the existence of the mobile π electrons and non-bonding electrons on the plenty of aromatized carbonic building blocks and presence of the surface decorative hetero atoms. From Fig. 5**a**, the prepared CQDs colloids exhibited broad band at 223 nm before dialysis, whereas, after dialysis a sharper and more intense photoluminescent emission band at 394 nm was detected. Similarly, from Fig. 5**b**, before dialysis a broad fluorescent band was detected at 281 nm, while after dialysis the fluorescent band become more intense and redder shifted to 493 nm (i.e., ranged in the green region) (Sasikala et al., 2016; Li et al., 2017; Yew et al., 2017).

The florescent properties of the nucleated CQDs are owing to the decorative functional groups that were inborn from MCC and well overlapped of π-π* and n-π* transitions for the aromatized nucleated CQDs (Sasikala et al., 2016; Li et al., 2017; Yew et al., 2017). In addition to, the surface decorative groups mainly effect on the location of absorption, resulting in the colorful appearance of CQDs colloids and endowing their easier colorimetric estimation. So, it could be summarized that, photoluminescence spectra of CQDs confirmed the geometrical characters and the fluorescence of CQDs ingrained from MCC. The optical activity data approved that the hydrothermally synthesized CQDs could emit in visible region so it has the ability of a strong fluorescent activity in visible range, which consequently facilitate their application in the biomedical purpose and could currently elaborate through the photoluminescence spectrum of CQDs.

3.5. Antitumor affinity of CQDs for tumor cells apoptosis

WST-1 Cell Proliferation Assay is ascribed as a colorimetric assay that is basically dependent on cleaving of tetrazolium salt (WST-1) by succinate-tetrazolium reductase that is belonging to the mitochondrial respiratory chain to liberate formazan dye in viable cell. Whereas, higher number of viable cells (metabolically active cells), higher are the amounts of liberated formazan. Therefore, by monitoring the addition of WST-1for detecting of the formazan level in the tested cells, it could be in turn be beneficial for quantification of the cells number. Thus, the amount of the resulted formazan is directly related to the number of metabolically active cells. In the current report, WST-1 assay was carried out for comparative studying of the anti-proliferative effects of CQDs prepared under hydrothermal conditions versus CQDs nucleated with infrared assisted technique on against Hepatocellular Carcinoma

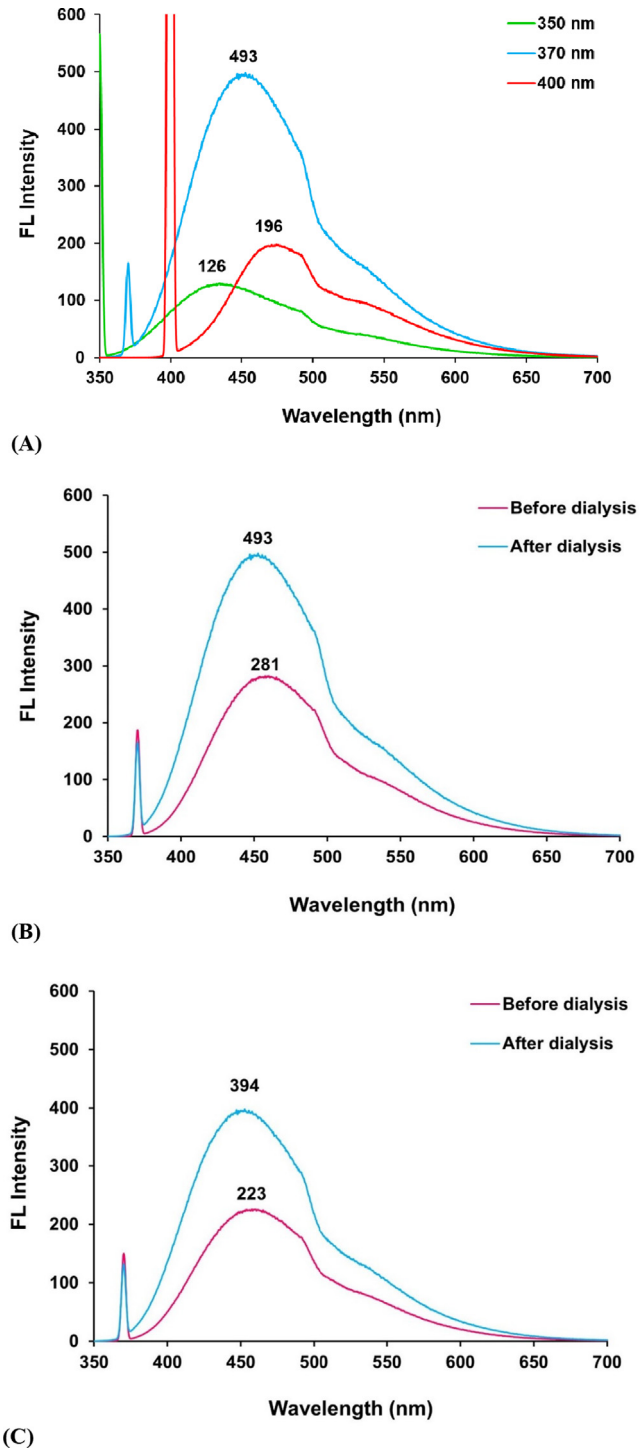

Fig. 5 **[A]** Excitation spectra for the hydrothermal synthesized CQDs after dialysis at different wavelength (350, 370, 400 nm). **[B, C]** Emission spectra (excitation wavelength length = 370 nm) for the synthesized CQDs before and after dialysis; **[B]** hydrothermal (HT) and **[C]** Infrared (IR).

(HepG2) cell line. The represented data showed that, treating of cancer cells with the as-prepared CQDs for 48 h resulted in increment in cell mortality percentage, whereas, higher cytotoxicity of the ingrained CQDs resulted in increment in the mortal cells, which subsequently decreased the resultant formazan dye and in turn decreasing the optical density. Therefore, following up the decrement of optical density was important for following up the increment in the number of mortal cells. **Figures S3** represented the optical density and cell mortality percentage in case of treating Hepatocellular Carcinoma (HepG2) cells with reference reagent (referred as formula) for cancer treatment, whereas the data showed that, with maximizing the formula concentration up to 1000 μg/mL the optical density was gradually decreased to reach 0.19, while, the cell mortality percentage was estimated to be 73.1 %. Fig. S3**c** is plotted for the effect of treating cancer cells with MCC, CQDs prepared under hydrothermal conditions (CQDs-HT) and CQDs nucleated with infrared assisted technique (CQDs-IR) on the optical density. Regardless to the applied technique, the currently prepared CQDs were exhibited with superior mortal action against the tested cancer cells, while, the treatment of the cancer cells with CQDs-HT resulted in much increment of the number of mortal cells, i.e., CQDs nucleated under hydrothermal conditions exhibited higher anticancer affinity. The plotted data depicted that, for treatment of the tested cancer cells with MCC, the optical density was insignificantly decreased. Whereas, in case of treating the tested cell line with CQDs-HT and CQDs-IR and with maximizing their concentration up to 1000 μg/mL, the optical density values were significantly decreased to reach 0.06 and 0.12, respectively.

Fig. S3**d** showed relation between the technique of synthesis for CQDs prepared from MCC and the cell mortality percent, as treatment of the examined cancer cells with CQDs-HT showed higher affinity to decrease the cell proliferation and increase the cell mortality percent of Hepatocellular Carcinoma (HepG2) cells by 3.5 % to 91.1 % compared to MCC as a blank (0.9 – 10.5 %) with maximizing the concentration from 10 up to 1000 μg/mL. Also, in case of exploiting CQDs-IR for treatment of Hepatocellular Carcinoma (HepG2) cells, it showed good anti-proliferative action, as the cell mortality percent was increased from 32 % to 83.0 %. These findings significantly approved that; CQDs-HT showed more affinity for cell mortality toward Hepatocellular Carcinoma (HepG2) cell line compared to CQDs-IR. Fig. S3**e** represented the estimated 50 % cytotoxic concentration (IC50) in μg/mL for formula, compared to the currently prepared CQDs-HT & CQDs-IR against the examined Hepatocellular Carcinoma (HepG2) cell line. It could be declared that, compared to formula (IC50 of 736.6 μg/mL), CQDs-HT exhibited with IC_{50} value of 378.2 μg/mL, while CQDs-IR showed IC50 value of 482.5 μg/mL. These findings also affirmed that, the cytotoxic effect of CQDs-HT on cancer cells was significantly higher with significant lower concentration rather than CQDs-IR.

The effect of any reagent for killing alive cell is known as cytotoxicity effect, while, such reagent is supposed to exhibit cell mortal effect via motivating the necrosis i.e., accidental cell mortality, or apoptosis i.e., programmed cell death. In accordance to literature (Arkan et al., 2018), apoptosis or the programmed cell-death is ascribed as a favorable mode of action for the antitumor reagents. Recent approaches were interestingly considered with the investigation of potential drugs for inducing the apoptosis in the malignant cell. The antitumor affinity and anti-proliferative action of the ingrained CQDs in the current report could be explained as follows (Fig. 6),

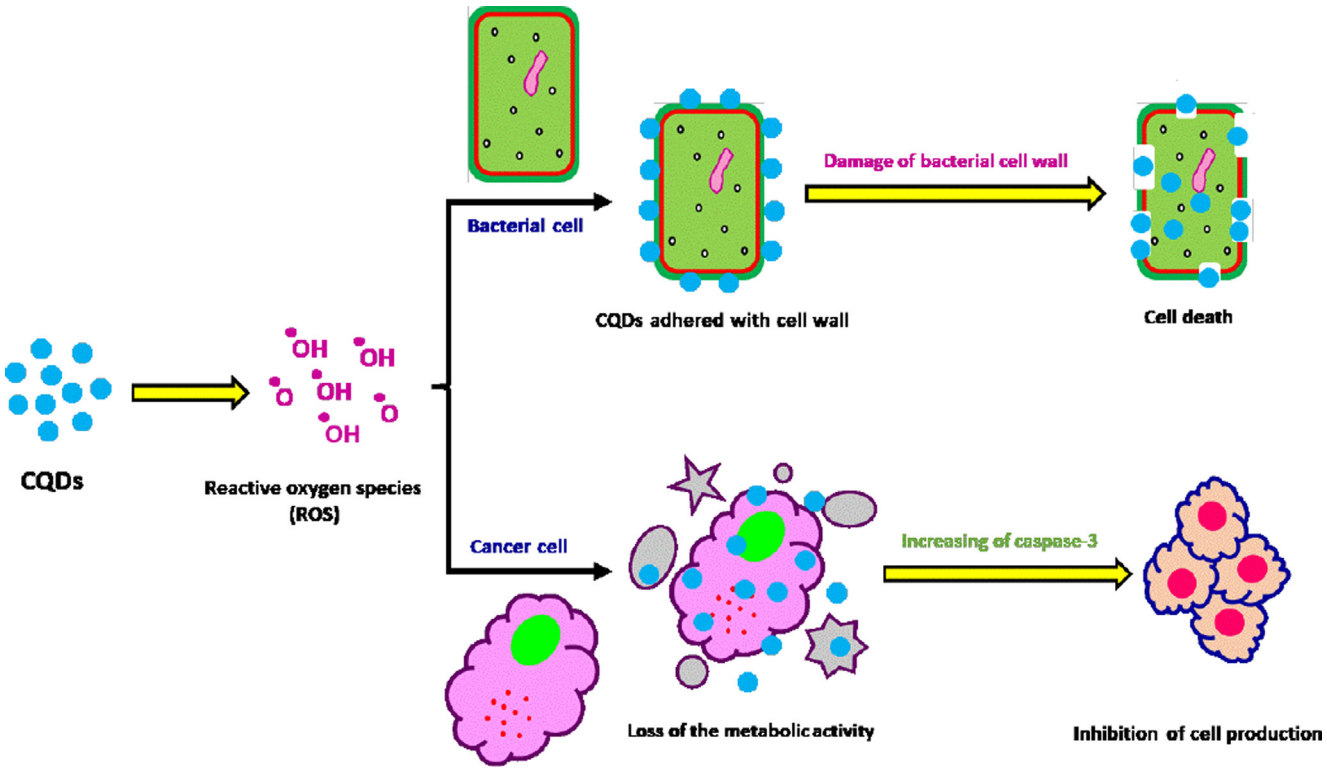

Fig. 6 The plausible mechanism of antibacterial and anticancer activity for the prepared CQDs.

i) Caspase-3 is one of end proteases, as it is identified as an enzyme that controls the apoptosis signal network and inflammation, while, it exhibits an essential role in damaging the cellular structure via degrading the cytoskeleton proteins or fragmenting nucleic acids (Elmore, 2007; Milner et al., 2002).
ii) activation of Caspase-3 is well-known to essentially act in motivating and progressing of apoptosis,
iii) the ingrained CQDs contained free mobile electrons that could inhibit the growth of the examined cancer cells via generation of reactive oxygen species (ROS) for activation of caspase-3.

So, it could be elucidated in summarization that, the treatment with the currently prepared CQDs was mainly acted in activating of caspase-3 of Hepatocellular Carcinoma (HepG2) cells, and consequently leading in apoptotic cell mortality.

3.6. Microbicide potency

It was approved that CQDs can superiorly exhibit microbicide potency against different bacterial strains (Li et al., 2018; Li et al., 2016; Ipe et al., 2005; Dong et al., 2020; Marković et al., 2018; Ristic et al., 2014; Stanković et al., 2018; Kováčová et al., 2018). In the current approach, via inhibition zone methodology, the microbicide potency for the ingrained CQDs was systematically studied against three different bacterial strains; gram positive bacterial strain (*Staph. aureus)*, gram negative bacterial strain (*E. coli*) and fungal strain (*C. albicans*). Additionally, CQDs minimal inhibitory concentration (MIC) was also estimated. The evaluated results were tabulated in Table 1, as it strongly revealed that, against all the examined bacterial and fungal strains, CQDs showed excellent microbicide potentiality. In case of dropping CQDs-HT colloid, the diameter of the inhibition zone in the plates prepared

Table 1 Antimicrobial activities of the synthesized CQDs.

Sample	Gram + ve bacteria	Gram -ve bacteria	Unicellular fungi
	Staphylococcus aureus	*Escherichia coli*	*Candida albicans*
MCC	0	0	0
CQDs-HT	14	17	13
CQDs-IR	12	14	12
MIC (μg/mL)			
MCC	> 1000	> 1000	> 1000
CQDs-HT	250	100	350
CQDs-IR	350	300	400

with *Staph. aureus, E. coli* and *C. albicans*, was estimated to be 12, 14 & 12 mm, respectively. Whereas, preparation of CQDs-IR was shown insignificant effects on the estimated data of inhibition zone to be 14, 17 & 13 mm for plates prepared with microbial strains of with *Staph. aureus, E. coli* & *C. albicans*, respectively.

The MIC of the as prepared CQDs was evaluated against *Staphy. aureus, E. coli* and *C. albicans* to be 250, 100 & 350 μL/mL, and 350, 300 & 400 μL/mL, for CQDs-HT and CQDs-IR, respectively. So, it could be depicted that, MIC was observably enhanced for CQDs-HT rather than CQDs-IR. The estimated data are in agreement with that reported in literature (Li et al., 2018; Dong et al., 2020; Ristic et al., 2014; Stanković et al., 2018; Kováčová et al., 2020) while the mechanism of their action as antimicrobial reagents could be simply ascribed as follows as suggested in Fig. 6;

i) Superiority of the currently ingrained CQDs as potent microbicidal laborer is essentially referred to their construction of decorative hydroxyl groups,
ii) Decorative oxygen containing groups are responsible for the mortal effects of the prepared CQDs against the tested microbial cells through the generation of reactive oxygen species (ROS),
iii) The liberated ROS acted in killing the microbial cells, as ROS were adhered then penetrated the microbial cell wall to act in motivating of the oxidative stress with deteriorating DNA & RNA, leading to inhibit and alter the gene expressions. Additionally, ROS act in the dysfunction of mitochondria, lipid per-oxidization, inactivating of intracellular protein, gradual degradation of the cell wall, and eventually leaded to apoptotic cell death.
iv) CQDs-HT showed significantly enhanced microbicide potentiality attributing to the effectiveness of hydrothermal conditions in nucleation of small and size controllable CQDs to be easily penetrated to the microbial cell wall for eventual cell mortality.

Comparing to metal-based nanomaterials and metal organic frameworks that were reported to exhibit microbicide potentiality and were recently studied in numerous reports (Emam et al., 2019; Emam et al., 2017; Ahmed et al., 2019; Emam et al., 2018), the currently prepared CQDs colloids were shown to exhibit significantly lower values of MIC. This could affirm the superior microbicide potency of the currently prepared CQDs, in addition to its biodegradability, low toxic effects and biocompatibility. Therefore, it could be favorably exploited as microbicide laborers rather than the metal-based nanomaterials for the biological and environmental related purposes.

4. Conclusion

Urgent requirement for medication from cancer diseases and different microbial infections are interestingly considered. Numerous approaches were concerned with investigation of easily synthesized therapeutic laborers with excellent affinity. CQDs as environmentally friendly fluorescent carbon nano-functionalized materials are popularly considered for application in medical purposes. Whereas, the synthetic methodology of carbon quantum dots (CQDs) affects their affinity and optical properties. Herein, a comparative study for the affinity of CQDs ingrained from microcrystalline cellulose (MCC) prepared under hydrothermal conditions (CQDs-HT) versus that prepared under infrared assisted technique (CQDs-IR) for acting as anticancer and antimicrobial laborers. Successive ingraining of CQDs via the exploitation of MCC under the hydrothermal versus infrared assisted techniques was individually affirmed via several instrumental analyses including UV–Visible spectroscopy, Transmission Electron Microscopy, FTIR, ^{1}H NMR and ^{13}C NMR. Afterword, the fluorescent properties of the ingrained CQDs were also followed up. The microbicide potency of the prepared CQDs was confirmed via inhibition zone method. Moreover, the anticancer potentiality of the synthesized CQDs was examined via WST-1 cell proliferation assay for monitoring their antitumor effects against Hepatocellular Carcinoma (HepG2) for CQDs prepared via hydrothermal (CQDs-HT) versus infrared assisted (CQDs-IR) techniques. All the illustrated data approved that, the currently prepared CQDs showed higher antiproliferative action against Hepatocellular Carcinoma (HepG2), moreover, it also exhibited with excellent microbicide potentiality, however, hydrothermal technique showed seniority over infrared assisted technique in nucleation of CQDs with higher anticancer and microbicide activities.

Declaration of Competing Interest

The authors declare that they have no known competing financial interests or personal relationships that could have appeared to influence the work reported in this paper.

Acknowledgements

The authors extend their appreciation to the Deanship for Research & Innovation, Ministry of Education in Saudi Arabia for funding this research work through the project number: IFP22UQU4350527DSR003.

Consent to Publish

Availability of data and materials

All data generated or analysed during this study are included in this published article (and its supplementary information files).

Appendix A. Supplementary material

Supplementary data to this article can be found online at https://doi.org/10.1016/j.arabjc.2022.104419.

References

Ahmed, H.B., Attia, M.A., El-Dars, F.M., Emam, H.E., 2019. Hydroxyethyl cellulose for spontaneous synthesis of antipathogenic nanostructures:(Ag & Au) nanoparticles versus Ag-Au nano-alloy. Int. J. Biol. Macromol. 128, 214–229.

Alaufi, O.M., Noorwali, A., Zahran, F., Al-Abd, A.M., Al-Attas, S., 2017. Cytotoxicity of thymoquinone alone or in combination with cisplatin (CDDP) against oral squamous cell carcinoma in vitro. Sci. Rep. 7 (1), 1–12.

Arkan, E., Barati, A., Rahmanpanah, M., Hosseinzadeh, L., Moradi, S., Hajialyani, M., 2018. Green synthesis of carbon dots derived from walnut oil and an investigation of their cytotoxic and

apoptogenic activities toward cancer cells. Adv. Pharma. Bull. 8 (1), 149.
Barati, A., Shamsipur, M., Arkan, E., Hosseinzadeh, L., Abdollahi, H., 2015. Synthesis of biocompatible and highly photoluminescent nitrogen doped carbon dots from lime: analytical applications and optimization using response surface methodology. Mater. Sci. Eng.: C 47, 325–332.
Chen, B., Li, F., Li, S., Weng, W., Guo, H., Guo, T., Zhang, X., Chen, Y., Huang, T., Hong, X., 2013. Large scale synthesis of photoluminescent carbon nanodots and their application for bioimaging. Nanoscale 5 (5), 1967–1971.
CLSI, Methods for Dilution Antimicrobial Susceptibility Tests for Bacteria That Grow Aerobically; Approved Standard—Ninth Edition, Vol. 32 No. 2, M07-A9 Clinical and Laboratory Standards Institute USA, 2012.
Dong, X., Liang, W., Meziani, M.J., Sun, Y.-P., Yang, L., 2020. Carbon dots as potent antimicrobial agents. Theranostics 10 (2), 671.
Dong, Y., Lin, J., Chen, Y., Fu, F., Chi, Y., Chen, G., 2014. Graphene quantum dots, graphene oxide, carbon quantum dots and graphite nanocrystals in coals. Nanoscale 6 (13), 7410–7415.
Elmore, S., 2007. Apoptosis: a review of programmed cell death. Toxicol. Pathol. 35 (4), 495–516.
Emam, H.E., Zahran, M., Ahmed, H.B., 2017. Generation of biocompatible nanogold using H2O2–starch and their catalytic/antimicrobial activities. Eur. Polym. J. 90, 354–367.
Emam, H.E., Darwesh, O.M., Abdelhameed, R.M., 2018. In-growth metal organic framework/synthetic hybrids as antimicrobial fabrics and its toxicity. Colloids Surf. B: Biointerfaces 165, 219–228.
Emam, H.E., Ahmed, H.B., El-Deib, H.R., El-Dars, F.M., Abdelhameed, R.M., 2019. Non-invasive route for desulfurization of fuel using infrared-assisted MIL-53 (Al)-NH2 containing fabric. J. Colloid Interface Sci. 556, 193–205.
Emam, H.E., Ahmed, H.B., 2021. Antitumor/antiviral carbon quantum dots based on carrageenan and pullulan. Int. J. Biol. Macromol. 170, 688–700.
Emam, H.E., El-Shahat, M., Hasanin, M.S., Ahmed, H.B., 2021. Potential military cotton textiles composed of carbon quantum dots clustered from 4–(2, 4–dichlorophenyl)–6–oxo–2–thioxohexahydropyrimidine–5–carbonitrile. Cellulose 28 (15), 9991–10011.
Fan, Z., Li, Y., Li, X., Fan, L., Zhou, S., Fang, D., Yang, S., 2014. Surrounding media sensitive photoluminescence of boron-doped graphene quantum dots for highly fluorescent dyed crystals, chemical sensing and bioimaging. Carbon 70, 149–156.
Gao, X., Du, C., Zhuang, Z., Chen, W., 2016. Carbon quantum dot-based nanoprobes for metal ion detection. J. Mater. Chem. C 4 (29), 6927–6945.
Hsu, P.-C., Chen, P.-C., Ou, C.-M., Chang, H.-Y., Chang, H.-T., 2013. Extremely high inhibition activity of photoluminescent carbon nanodots toward cancer cells. J. Mater. Chem. B 1 (13), 1774–1781.
Ipe, B.I., Lehnig, M., Niemeyer, C.M., 2005. On the generation of free radical species from quantum dots. Small 1 (7), 706–709.
Kim, Y.J., Guo, P., Schaller, R.D., 2019. Aqueous carbon quantum dot-embedded PC60-PC61BM nanospheres for ecological fluorescent printing: contrasting fluorescence resonance energy-transfer signals between watermelon-like and random morphologies. J. Phys. Chem. Lett. 10 (21), 6525–6535.
M.r. Kováčová, Z.M. Marković, P. Humpolíček, M. Mičušík, H. Švajdlenková, A. Kleinová, M. Danko, P. Kubát, J. Vajďák, Z. Capakova, Carbon quantum dots modified polyurethane nanocomposite as effective photocatalytic and antibacterial agents, ACS Biomaterials Science & Engineering 4(12) (2018) 3983-3993.
Kováčová, M., Špitalská, E., Markovic, Z., Špitálský, Z., 2020. Carbon quantum dots as antibacterial photosensitizers and their polymer nanocomposite applications. Part. Part. Syst. Char. 37 (1), 1900348.
Kumar, S., Negi, Y.S., Upadhyaya, J.S., 2010. Studies on characterization of corn cob based nanoparticles. Adv. Mater. Lett. 1 (3), 246–253.
Kwon, W., Do, S., Rhee, S.-W., 2012. Formation of highly luminescent nearly monodisperse carbon quantum dots via emulsion-templated carbonization of carbohydrates. RSC Adv. 2 (30), 11223–11226.
Li, Y.J., Harroun, S.G., Su, Y.C., Huang, C.F., Unnikrishnan, B., Lin, H.J., Lin, C.H., Huang, C.C., 2016. Synthesis of self-assembled spermidine-carbon quantum dots effective against multidrug-resistant bacteria. Adv. Healthcare Mater. 5 (19), 2545–2554.
Li, H., He, X., Kang, Z., Huang, H., Liu, Y., Liu, J., Lian, S., Tsang, C.H.A., Yang, X., Lee, S.T., 2010. Water-soluble fluorescent carbon quantum dots and photocatalyst design. Angew. Chem. 122 (26), 4532–4536.
Li, H., Ming, H., Liu, Y., Yu, H., He, X., Huang, H., Pan, K., Kang, Z., Lee, S.-T., 2011. Fluorescent carbon nanoparticles: electrochemical synthesis and their pH sensitive photoluminescence properties. New J. Chem. 35 (11), 2666–2670.
Li, H., He, X., Liu, Y., Huang, H., Lian, S., Lee, S.-T., Kang, Z., 2011. One-step ultrasonic synthesis of water-soluble carbon nanoparticles with excellent photoluminescent properties. Carbon 49 (2), 605–609.
Li, H., Huang, J., Song, Y., Zhang, M., Wang, H., Lu, F., Huang, H., Liu, Y., Dai, X., Gu, Z., 2018. Degradable carbon dots with broad-spectrum antibacterial activity. ACS Appl. Mater. Interfaces 10 (32), 26936–26946.
Li, D., Na, X., Wang, H., Xie, Y., Cong, S., Song, Y., Xu, X., Zhu, B.-W., Tan, M., 2018. Fluorescent carbon dots derived from Maillard reaction products: their properties, biodistribution, cytotoxicity, and antioxidant activity. J. Agric. Food. Chem. 66 (6), 1569–1575.
Li, M., Yu, C., Hu, C., Yang, W., Zhao, C., Wang, S., Zhang, M., Zhao, J., Wang, X., Qiu, J., 2017. Solvothermal conversion of coal into nitrogen-doped carbon dots with singlet oxygen generation and high quantum yield. Chem. Eng. J. 320, 570–575.
Lim, S.Y., Shen, W., Gao, Z., 2015. Carbon quantum dots and their applications. Chem. Soc. Rev. 44 (1), 362–381.
Luo, Z., Lu, Y., Somers, L.A., Johnson, A.C., 2009. High yield preparation of macroscopic graphene oxide membranes. J. Am. Chem. Soc. 131 (3), 898–899.
Marković, Z.M., Jovanović, S.P., Mašković, P.Z., Danko, M., Mičušík, M., Pavlović, V.B., Milivojević, D.D., Kleinová, A., Špitalský, Z., Marković, B.M.T., 2018. Photo-induced antibacterial activity of four graphene based nanomaterials on a wide range of bacteria. RSC Adv. 8 (55), 31337–31347.
Milner, A., Palmer, D., Hodgkin, E., Eliopoulos, A., Knox, P., Poole, C., Kerr, D., Young, L., 2002. Induction of apoptosis by chemotherapeutic drugs: the role of FADD in activation of caspase-8 and synergy with death receptor ligands in ovarian carcinoma cells. Cell Death Differ. 9 (3), 287–300.
Pandey, F.P., Rastogi, A., Singh, S., 2020. Optical properties and zeta potential of carbon quantum dots (CQDs) dispersed nematic liquid crystal 4′-heptyl-4-biphenylcarbonitrile (7CB). Opt. Mater. 105, 109849.
Pidot, S.J., Gao, W., Buultjens, A.H., Monk, I.R., Guerillot, R., Carter, G.P., Lee, J.Y., Lam, M.M., Grayson, M.L., Ballard, S.A., 2018. Increasing tolerance of hospital Enterococcus faecium to handwash alcohols. Sci. Transl. Med. 10 (452), eaar6115.
Qu, S., Wang, X., Lu, Q., Liu, X., Wang, L., 2012. A biocompatible fluorescent ink based on water-soluble luminescent carbon nanodots. Angew. Chem. 124 (49), 12381–12384.
Ristic, B.Z., Milenkovic, M.M., Dakic, I.R., Todorovic-Markovic, B. M., Milosavljevic, M.S., Budimir, M.D., Paunovic, V.G., Dramicanin, M.D., Markovic, Z.M., Trajkovic, V.S., 2014. Photodynamic antibacterial effect of graphene quantum dots. Biomaterials 35 (15), 4428–4435.

Ryu, J., Suh, Y.-W., Suh, D.J., Ahn, D.J., 2010. Hydrothermal preparation of carbon microspheres from mono-saccharides and phenolic compounds. Carbon 48 (7), 1990–1998.

Sachdev, A., Gopinath, P., 2015. Green synthesis of multifunctional carbon dots from coriander leaves and their potential application as antioxidants, sensors and bioimaging agents. Analyst 140 (12), 4260–4269.

Sakaki, T., Shibata, M., Miki, T., Hirosue, H., Hayashi, N., 1996. Reaction model of cellulose decomposition in near-critical water and fermentation of products. Bioresour. Technol. 58 (2), 197–202.

Sasikala, S.P., Henry, L., Yesilbag Tonga, G., Huang, K., Das, R., Giroire, B., Marre, S., Rotello, V.M., Penicaud, A., Poulin, P., 2016. High yield synthesis of aspect ratio controlled graphenic materials from anthracite coal in supercritical fluids. ACS Nano 10 (5), 5293–5303.

Sharma, A., Marceau, C., Hamaguchi, R., Burridge, P.W., Rajarajan, K., Churko, J.M., Wu, H., Sallam, K.I., Matsa, E., Sturzu, A.C., 2014. Human induced pluripotent stem cell–derived cardiomyocytes as an in vitro model for coxsackievirus B3–induced myocarditis and antiviral drug screening platform. Circ. Res. 115 (6), 556–566.

N.K. Stanković, M. Bodik, P. Šiffalovič, M. Kotlar, M. Mičušik, Z. Špitalsky, M. Danko, D.a.D. Milivojević, A. Kleinova, P. Kubat, Antibacterial and antibiofouling properties of light triggered fluorescent hydrophobic carbon quantum dots Langmuir–Blodgett thin films, ACS Sustainable Chemistry & Engineering 6(3) (2018) 4154-4163.

Sun, Y.-P., Zhou, B., Lin, Y., Wang, W., Fernando, K.S., Pathak, P., Meziani, M.J., Harruff, B.A., Wang, X., Wang, H., 2006. Quantum-sized carbon dots for bright and colorful photoluminescence. J. Am. Chem. Soc. 128 (24), 7756–7757.

Vasimalai, N., Vilas-Boas, V., Gallo, J., de Fátima Cerqueira, M., Menéndez-Miranda, M., Costa-Fernández, J.M., Diéguez, L., Espiña, Fernández-Argüelles, M.T., 2018. Green synthesis of fluorescent carbon dots from spices for in vitro imaging and tumour cell growth inhibition. Beilstein J. Nanotechnol. 9 (1), 530–544.

Wang, Y., Hu, A., 2014. Carbon quantum dots: synthesis, properties and applications. J. Mater. Chem. C 2 (34), 6921–6939.

Wang, R., Lu, K.-Q., Tang, Z.-R., Xu, Y.-J., 2017. Recent progress in carbon quantum dots: synthesis, properties and applications in photocatalysis. J. Mater. Chem. A 5 (8), 3717–3734.

Wu, Z.L., Zhang, P., Gao, M.X., Liu, C.F., Wang, W., Leng, F., Huang, C.Z., 2013. One-pot hydrothermal synthesis of highly luminescent nitrogen-doped amphoteric carbon dots for bioimaging from Bombyx mori silk–natural proteins. J. Mater. Chem. B 1 (22), 2868–2873.

Wu, Z.L., Gao, M.X., Wang, T.T., Wan, X.Y., Zheng, L.L., Huang, C.Z., 2014. A general quantitative pH sensor developed with dicyandiamide N-doped high quantum yield graphene quantum dots. Nanoscale 6 (7), 3868–3874.

Xu, X., Zhang, K., Zhao, L., Li, C., Bu, W., Shen, Y., Gu, Z., Chang, B., Zheng, C., Lin, C., 2016. Aspirin-based carbon dots, a good biocompatibility of material applied for bioimaging and anti-inflammation. ACS Appl. Mater. Interfaces 8 (48), 32706–32716.

Yew, Y.T., Loo, A.H., Sofer, Z., Klímová, K., Pumera, M., 2017. Coke-derived graphene quantum dots as fluorescence nanoquencher in DNA detection. Appl. Mater. Today 7, 138–143.

B. Zhang, C.y. Liu, Y. Liu, A novel one-step approach to synthesize fluorescent carbon nanoparticles, European Journal of Inorganic Chemistry 2010(28) (2010) 4411-4414.

Zhao, S., Lan, M., Zhu, X., Xue, H., Ng, T.-W., Meng, X., Lee, C.-S., Wang, P., Zhang, W., 2015. Green synthesis of bifunctional fluorescent carbon dots from garlic for cellular imaging and free radical scavenging. ACS Appl. Mater. Interfaces 7 (31), 17054–17060.